# Sensors & Diagnostics

Accepted Manuscript

This article can be cited before page numbers have been issued, to do this please use: K. Okutani, K. Imato and Y. Ooyama, *Sens. Diagn.*, 2026, DOI: 10.1039/D6SD00055J.




ROYAL SOCIETY OF CHEMISTRY

rsc.li/sensors

View Article Online
DOI: 10.1039/D6SD00055J

ARTICLE

# Development of colorimetric and fluorescent sensor based on a combination of ICT (intramolecular charge transfer) and FRET (Förster resonance energy transfer) for detection of water

Received 00th January 20xx,
Accepted 00th January 20xx

DOI: 10.1039/x0xx00000x

Kosuke Okutani, Keiichi Imato and Yousuke Ooyama*

Colorimetric and fluorescent sensors for water are crucial to environmental and quality control monitoring, industrial process, food inspection and so on. Although the optical sensing mechanism of sensors for water has been of considerable concern in analytical chemistry, photochemistry, and photophysics in recent years, a further fundamental study is necessary to provide a direction in molecular design toward creating the highly sensitive fluorescent sensor for detecting, quantitating and visualizing a trace amount of water in solids, liquids, or gases. In this work, we have newly designed and synthesized a ICT (intramolecular charge transfer)/FRET (Förster resonance energy transfer)-type colorimetric and fluorescent sensor, pyridine-boron trifluoride complex **KOY-1-BF$_3$**, where thienylpyridine-carbazole-based D-(π-A)$_2$ skeleton and boron-dipyrromethene (BODIPY) skeleton are the ICT-type donor fluorophore and the acceptor fluorophore in the FRET process, respectively. It was found that the addition of water to **KOY-1-BF$_3$** solution causes its dissociation into thienylpyridine-carbazole-based D-(π-A)$_2$ fluorophore **KOY-1** and then the energy transfer from thienylpyridine-carbazole-based D-(π-A)$_2$ skeleton to BODIPY skeleton through the FRET process, and thus resulting in a large pseudo-Stokes shift of 7942 cm$^{-1}$ (150 nm) and an enhancement of fluorescence emission originating from BODIPY skeleton as well as the blue-shift of ICT-based photoabsorption band. Furthermore, in the high water content region, a decrease in the fluorescence intensity was observed due to the formation of hydrogen-bonded proton transfer complex **KOY-1-H$_2$O** with water molecules which shows a feeble fluorescence emission property, leading to low FRET efficiency. Consequently, this work is the first report on the development and optical sensing mechanism of ICT/FRET-type colorimetric and fluorescent fluorescence sensor for water possessing large pseudo-Stokes shift.

## Introduction

Development of techniques for detecting and quantitating a trace amount of water in solids, liquids, or gases is absolutely essential for not only environmental and quality control monitoring systems and industry, but for establishing new principles in chemistry, chemical engineering, and physics. In fact, various water content measurement techniques based on chromatographic, chemical, electrical, thermogravimetric, or electromagnetic methods have been developed and are widely used in laboratory, industry, and everyday life.[1, 2] On the other hand, if we can create optical methods using colorimetric and fluorescent sensors for water, the technique allows us not only to perform quick flow analysis with sufficient accuracy and high sensitivity, but also to visually confirm the presence of water in samples and on material surfaces.[3–15] For this purpose, various types of colorimetric and fluorescent sensors for water have been designed and developed, based on ICT (intramolecular charge transfer),[16–23] ESIPT (excited state intramolecular proton transfer),[24–27] PET (photo-induced electron transfer),[28–44] FRET (Förster resonance energy transfer)[45, 46] or solevatofluorochromism (SFC)[47–53] characteristics, which exhibit the photophysical changes in wavelength, intensity, and lifetime of photoabsorption and photoluminescence depending on the water content. Among them, the ICT-type and FRET-type fluorescent sensors make it possible to the colorimetric and ratiometric fluorescent measurements which are preferable because the ratio of the photoabsorption and fluorescence intensities at the two wavelengths is independent of the total concentration of the sensor, photobleaching, fluctuations of light source intensity, sensitivity of the instrument, and so on.[54–60] The ICT-type fluorescent sensors have generally donor-π-acceptor (D-π-A) structure which are composed of an electron-donating (D) moiety and an electron-accepting (A) moiety linked by a π-conjugated bridge, so that they exhibit an intense photoabsorption band originating from the ICT characteristics from the D to the A moiety. In our previous work, in order to gain insight into a direction in molecular design toward creating the ICT-type colorimetric and fluorescent sensor for detection of water in solvents, we have designed and developed a D-(π-A)$_2$-type pyridine-boron trifluoride complex **YNI-2-BF$_3$** composed of a two thienyl carbazole skeleton as D-π moiety and two pyridine-boron trifluoride units as A moiety (Fig. 1).[19] In the low water content region, **YNI-2-BF$_3$** exhibited a decrease in the

*Applied Chemistry Program, Graduate School of Advanced Science and Engineering, Hiroshima University, 1-4-1 Kagamiyama, Higashi-Hiroshima 739-8527, Japan. E-mail: yooyama@hiroshima-u.ac.jp*
Electronic Supplementary Information (ESI) available. See DOI: 10.1039/x0xx00000x

ICT-based photoabsorption band with a simultaneous increase in another ICT-based photoabsorption band in shorter-wavelength, and the appearance and enhancement of a fluorescence emission band, which is attributed to the change in the ICT characteristics due to the dissociation of **YNI-2-BF$_3$** into D-(π-A)$_2$-type pyridine dye **YNI-2**. Furthermore, in the relatively high water content region, a decrease in the fluorescence intensity was observed due to the formation of the hydrogen-bonded proton transfer complex (PTC) **YNI-2-H$_2$O** with water molecules which shows a feeble fluorescence emission property. However, the disadvantage in this ICT-based fluorescence sensing system for water is that the accuracy and sensitivity for detection and quantification of water is low due to self-quenching and fluorescence detection errors due to a strong spectral overlap between the ICT-based photoabsorption band of **YNI-2-BF$_3$** and the fluorescence band of **YNI-2**. Meanwhile, in FRET-based fluorescent sensors, the fluorescence emission originates from the acceptor fluorophore via an energy transfer process, that is, FRET process between the photoexcited donor fluorophore and the ground state acceptor fluorophore. Therefore, to achieve effective FRET, a strong overlap between the fluorescence emission spectrum of the donor fluorophore and the photoabsorption spectrum of the acceptor fluorophore is required. The most advantageous features of FRET-type fluorescent sensors is the large pseudo-Stokes shift (SS) between the photoabsorption maximum of donor fluorophore and the fluorescence maximum of acceptor fluorescence, which leads to an effective avoidance of the self-quenching and fluorescence detection errors due to photoexcitation and scattering lights from the excitation source.

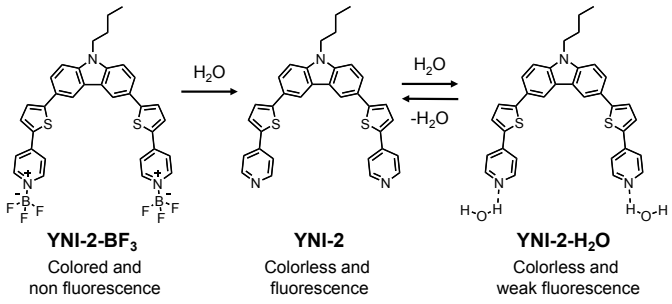


**Fig. 1** Proposed mechanisms of ICT-type colorimetric and fluorescent sensor **YNI-2-BF$_3$** for the detection of water in solvent (our previous work).[19]

Thus, in this work, in order to provide a direction in molecular design toward creating a ratiometric fluorescent sensor possessing large SS for detection of water over a wide range from low water content to high water content in solvents, we have newly designed and synthesized a ICT/FRET-type fluorescent sensor, pyridine-boron trifluoride complex **KOY-1-BF$_3$**, where the thienylpyridine-carbazole-based D-(π-A)$_2$ skeleton and boron-dipyrromethene (BODIPY) skeleton are the ICT-type donor fluorophore and the acceptor fluorophore in the FRET process, respectively (Fig. 2). It is expected that the addition of water to **KOY-1-BF$_3$** solution causes its dissociation into thienylpyridine-carbazole-based D-(π-A)$_2$-BODIPY fluorophore **KOY-1** and then the energy transfer from thienylpyridine-carbazole-based D-(π-A)$_2$ skeleton to BODIPY skeleton through the FRET process, and thus resulting in a large pseudo-SS and an enhancement of fluorescence emission originating from BODIPY skeleton. Moreover, in the relatively high water content region, it may induce the formation of the hydrogen-bonded proton transfer complex (PTC) **KOY-1-H$_2$O** with water molecules which shows a feeble fluorescence emission property, leading to a decrease in the fluorescence intensity due to low FRET efficiency. Indeed, this is the first report on the development and optical sensing mechanism of ICT/FRET-type colorimetric and fluorescent sensor for water, although some ICT/FRET-type fluorescent sensors for $H_2O_2$, $H_2S$ and cation species including $Cu^{2+}$ and $Zn^{2+}$ have been developed.[54–60] Herein, we provide the most promising fluorescence enhancement (turn-on) system for detecting, quantitating and visualizing water.

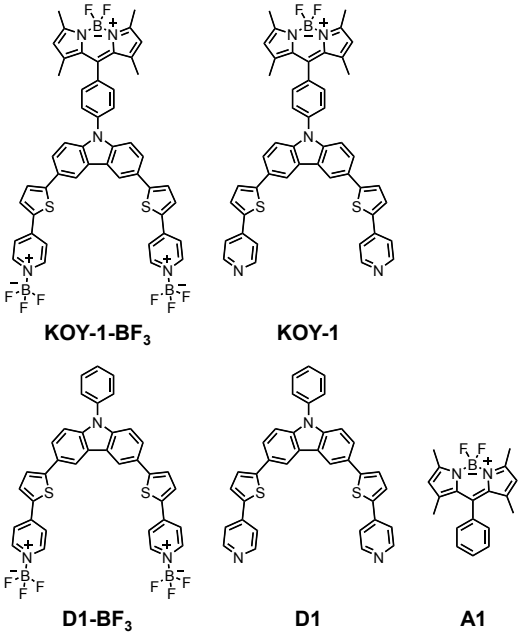


**Fig. 2** ICT/FRET-type fluorescent sensor **KOY-1-BF$_3$**, BODIPY/D-(π-A)$_2$-type fluorophore **KOY-1**, D-(π-A)$_2$-type pyridine-boron trifluoride complex **D1-BF$_3$**, and donor fluorophore **D1** and acceptor fluorophore **A1** in FRET process.

## Results and discussion

### Synthesis

The ICT/FRET-type fluorescent sensor **KOY-1-BF$_3$** was synthesized according to a stepwise synthetic protocol (Scheme 1). Compound **1** was prepared according to a reported procedure.[61] Compound **2** was obtained by bromination of compound **1** with *N*-bromosuccinimide (NBS). Compound **3** was obtained by the Stille coupling reaction of compound **2** with (tributylstannyl)thienylpyridine **S1**[62]. Dipyrromethane derivative **4** was prepared by condensation of compound **3** with 2,4-dimethylpyrrole. BODIPY/D-(π-A)$_2$-type fluorophore **KOY-1** was prepared by oxidation of compound **4** with 2,3-dichloro-5,6-dicyano-1,4-benzoquinone (DDQ) followed by treatment with with $BF_3$-$OEt_2$. Finally, ICT/FRET-type

fluorophore **KOY-1-BF$_3$** was obtained by treating **KOY-1** with $BF_3$-$OEt_2$ and fully characterized by $^1$H NMR, $^{11}$B NMR, FT-IR, high-resolution mass analysis, and thermogravimetry-differential thermal analysis (TG-DTA), although it was not possible to obtain the $^{13}$C NMR spectrum to make assignments due to the low solubility of **KOY-1-BF$_3$** in the solvent. In addition, the D-(π-A)$_2$-type compound **D1** as a donor fluorophore and its pyridine-boron trifluoride complex **D1-BF$_3$** were prepared (Fig. 1, see Scheme S1 for the synthesis, ESI†) and commercially available BODIPY **A1** was used as an acceptor fluorophore, where **D1-BF$_3$** and **A1** are structural components for **KOY-1-BF$_3$**.

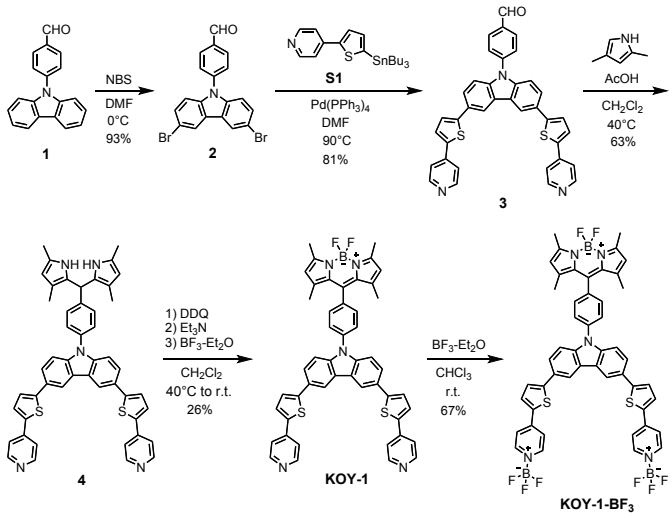


**Scheme 1** Synthesis of **KOY-1-BF$_3$**.

### Photoabsorption and fluorescence properties

The photoabsorption and fluorescence spectra of **D1-BF$_3$**, **A1**, **KOY-1**, and **KOY-1-BF$_3$** in acetonitrile and **D1** in THF (because **D1** is poor solubility in acetonitrile) are shown in Fig. 3. **D1** and **D1-BF$_3$** show a strong photoabsorption band in the ranges of 300 nm to 420 nm and 400 nm to 500 nm, respectively, which is assigned to the ICT excitation from the electron-donating moiety (carbazole skeleton) to the electron-accepting moiety (pyridyl groups for **D1** and pyridyne-$BF_3$ units for **D1-BF$_3$**). The ICT-based photoabsorption maximum ($\lambda^{abs}_{max}$ = 440 nm) of **D1-BF$_3$** occurs at a longer wavelength by 68 nm than that ($\lambda^{abs}_{max}$ = 372 nm) of **D1**, which could be due to the stronger electron-withdrawing ability of pyridyne-$BF_3$ unit than pyridyl group. The molar extinction coefficient ($\varepsilon_{max}$) for the ICT-based $\lambda^{abs}_{max}$ (440 nm) of **D1-BF$_3$** is 46400 $M^{-1}$ $cm^{-1}$, which is equivalent to that (52800 $M^{-1}$ $cm^{-1}$) of **D1**. **A1** shows a strong photoabsorption band ($\lambda^{abs}_{max}$ = 497 nm, $\varepsilon_{max}$ = 84700 $M^{-1}$ $cm^{-1}$) in the ranges of 420 nm to 520 nm originating from the BODIPY skeleton and a feeble and broad photoabsorption band in the range of 300 nm to 400 nm. On the other hand, **KOY-1** and **KOY-1-BF$_3$** show two strong photoabsorption bands in the ranges of 300 nm to 420 nm ($\lambda^{abs}_{max}$ = 366 nm, $\varepsilon_{max}$ = 53100 $M^{-1}$ $cm^{-1}$ for **KOY-1**) or 400 nm to 480 nm ($\lambda^{abs}_{max}$ = 441 nm, $\varepsilon_{max}$ = 50800 $M^{-1}$ $cm^{-1}$ for **KOY-1-BF$_3$**) and 480 nm to 520 nm ($\lambda^{abs}_{max}$ = 498 nm, $\varepsilon_{max}$ = 67600 $M^{-1}$ $cm^{-1}$ for **KOY-1** and $\lambda^{abs}_{max}$ = 498 nm, $\varepsilon_{max}$ = 64600 $M^{-1}$ $cm^{-1}$ for **KOY-1-BF$_3$**); the former and later are assigned to the ICT excitation from the electron-donating moiety (carbazole skeleton) to the electron-accepting moiety (pyridyl groups for **KOY-1** and pyridyne-$BF_3$ units for **KOY-1-BF$_3$**) and the BODIPY skeleton, respectively. For the corresponding fluorescence spectra, **D1** shows a fluorescence band with fluorescence maximum ($\lambda^{fl}_{max}$) at 457 nm in the ranges of 420 nm to 550 by a photoexcitation at 400 nm. For **D1-BF$_3$**, on the other hand, there is no detectable fluorescence spectrum. **A1** exhibits a $\lambda^{fl}_{max}$ at 514 nm originating from the BODIPY skeleton by the photoexcitation at 400 nm as well as 470 nm. It is worth mentioning here that the photoabsorption spectrum (420−520 nm) of acceptor fluorophore **A1** has spectral overlap with the fluorescence spectrum (420−550 nm) of donor fluorophore **D1** (Fig. S28, ESI†). The fact suggests that for **KOY-1** the FRET from the D-(π-A)$_2$ skeleton as the donor fluorophore to the BODIPY skeleton as the acceptor fluorophore occurs by the photoexcitation using the ICT-based $\lambda^{abs}_{max}$ of the D-(π-A)$_2$ skeleton (**D1** moiety), leading to fluorescence emission originating from the BODIPY skeleton. In fact, **KOY-1** exhibits two fluorescence bands with the $\lambda^{fl}_{max}$ at 450 nm and the $\lambda^{fl}_{max}$ at 516 nm originating from the D-(π-A)$_2$ skeleton and the BODIPY skeleton, respectively, by the photoexcitation ($\lambda^{ex}$ = 400 nm) corresponding to both the ICT-based photoabsorption of D-(π-A)$_2$ skeleton and the feeble and broad photoabsorption band of the BODIPY skeleton, although **KOY-1** shows an only fluorescence band with the $\lambda^{fl}_{max}$ at 515 nm originating from the BODIPY skeleton by the photoexcitation ($\lambda^{ex}$ = 470 nm) of the BODIPY skeleton (Fig. S26a, ESI†). However, this result indicates that the FRET efficiency for **KOY-1** is not quantitative by the fact that the two fluorescence bands originating from both the D-(π-A)$_2$ skeleton and the BODIPY skeleton were observed. Thus, we estimated the FERT efficiency for **KOY-1** from the equation $E_{FRET} = 1- (\tau_{DA}/\tau_D)$ based on time-resolved fluorescence lifetime measurements, where $\tau_{DA}$ and $\tau_D$ are the donor fluorescence lifetimes in the presence and absence of an acceptor, that is, $\tau_{DA}$ and $\tau_D$ are the fluorescence lifetimes of **KOY-1** (0.96 ns) and **D1** (1.70 ns), respectively, in acetonitrile. The FRET efficiency ($E_{FRET}$ value) for **KOY-1** in the absolute acetonitrile solution was evaluated to be 44%. The reason for the low $E_{FRET}$ value of **KOY-1** might be not only intense fluorescence emission originating from the D-(π-A)$_2$ skeleton (actually, the fluorescent quantum yield $\Phi_{fl}$ of **D1** is 76% in absolute acetonitrile) that is too strong for the BODIPY skeleton to well absorb the energy, but also poor overlap integral of the donor fluorescence spectrum with the acceptor photoabsorption spectrum. Meanwhile, **KOY-1-BF$_3$** exhibits an only fluorescence band with the $\lambda^{fl}_{max}$ at 517 nm originating from the BODIPY skeleton by both the photoexcitation ($\lambda^{ex}$ = 400 nm) of the D-(π-A)$_2$ and BODIPY skeletons and the photoexcitation ($\lambda^{ex}$ = 470 nm) of only the BODIPY skeleton (Fig. S26c, ESI†), which is not due to the FRET process but due to the photoexcitation of the BODIPY skeleton because the **D1-BF$_3$** skeleton exhibits no fluorescence emission. Nevertheless, it is expected that the addition of water to **KOY-1-BF$_3$** solution causes its dissociation into thienylpyridine-carbazole-based D-(π-A)$_2$ fluorophore **KOY-1** and then the energy transfer from the

D-(π-A)$_2$ skeleton to the BODIPY skeleton through the FRET process, and thus resulting in the enhancement of fluorescence emission originating from BODIPY skeleton. In addition, it was found the pseudo-SS value of **KOY-1** between the $\lambda^{abs}_{max}$ of the D-(π-A)$_2$ skeleton and the $\lambda^{fl}_{max}$ of the BODIPY skeleton is 7942 cm$^{-1}$ (150 nm), which is significantly higher than that (5000 cm$^{-1}$; 85 nm) of **D1** and that (665 cm$^{-1}$; 17 nm) of **A1**.

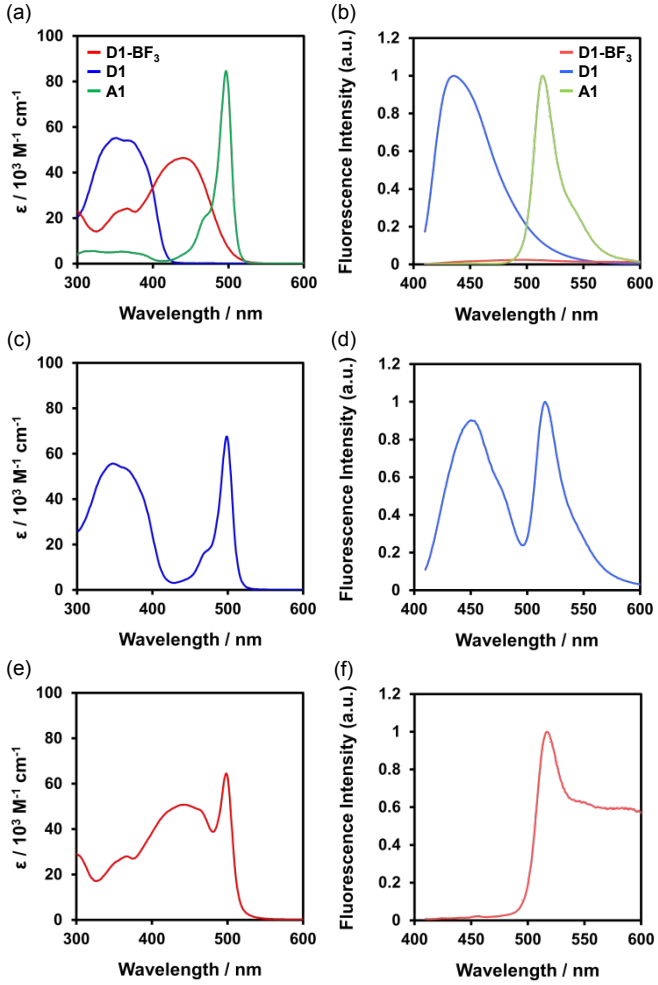


**Fig. 3** (a) Photoabsorption and (b) fluorescence ($\lambda^{ex}$ = 400 nm) spectra of **D1** ($c$ = 2.0×10$^{-5}$ M) in THF, **D1-BF$_3$** ($c$ = 2.0×10$^{-5}$ M), and **A1** ($c$ = 2.0×10$^{-5}$ M) in acetonitrile. (c) Photoabsorption and (d) fluorescence ($\lambda^{ex}$ = 400 nm) spectra of **KOY-1** ($c$ = 2.0×10$^{-5}$ M) in acetonitrile. (e) Photoabsorption and (f) fluorescence ($\lambda^{ex}$ = 400 nm) spectra of **KOY-1-BF$_3$** ($c$ = 2.0×10$^{-5}$ M) in acetonitrile.

### Optical sensing ability for water

In order to investigate the optical sensing ability of **KOY-1-BF$_3$** for water in a solvent, the photoabsorption and fluorescence spectra of **D1**, **D1-BF$_3$**, **A1** and **KOY-1** as well as **KOY-1-BF$_3$** were measured in acetonitrile or THF containing various concentrations of water (Fig. 4). For **KOY-1-BF$_3$**, the ICT-based photoabsorption band at around 440 nm decreases with the simultaneous increase in a photoabsorption band at around 360 nm which is assignable to the ICT-based photoabsorption band of **KOY-1** with the increase in the water content in acetonitrile solution (Fig. 4a, c). On the other hand, the photoabsorption band at around 500 nm originating from the BODIPY skeleton show unnoticeable changes upon addition of water to the acetonitrile solution. The decrease and increase in the two ICT-based photoabsorption bands level off in the water content region greater than 40 wt%, but it should be noticed that the existence of isosbestic point was not observed in the water content range from 0.0099 wt% (absolute acetonitrile) to 40 wt% (Fig. 4a inset), although the absorbance at around 400 nm does not appear to change. Thus, the absence of isosbestic point indicates the presence of the three or more chemical species, that is, the two or more reactions and equilibriums occur upon addition of water to the sensor solution.[63, 64] The corresponding fluorescence spectra of **KOY-1-BF$_3$** exhibited the appearance and enhancement of a fluorescence emission band at around 460 nm as well as the enhancement of fluorescence emission intensity at around 515 nm originating from the BODIPY skeleton in the water content region below 25 wt%, and then underwent a decrease in the intensity of both the fluorescence emission bands in the water content region over 30 wt% (Fig. 4b, d). Actually, for **KOY-1-BF$_3$** in acetonitrile solution containing water content of 25 wt%, the photoabsorption spectrum (420−520 nm) originating from the BODIPY skeleton has spectral overlap with the fluorescence spectrum (420−550 nm) originating from D-(π-A)$_2$ skeleton. (Fig. S28, ESI†). The fact strongly indicated that the addition of water to **KOY-1-BF$_3$** solution causes its dissociation into thienylpyridine-carbazole-based D-(π-A)$_2$ fluorophore **KOY-1** and then the FRET process from the excited-state donor fluorophore D-(π-A)$_2$ skeleton to acceptor fluorophore BODIPY skeleton. In fact, it was confirmed that removing water from **KOY-1-BF$_3$** acetonitrile solution containing water does not recover to the original **KOY-1-BF$_3$**. Meanwhile, as with the case of **YNI-2**, the photoabsorption spectra of **D1** showed a slight bathochromic shift upon addition of water to the THF solution (Fig. S27a, c, ESI†). The corresponding fluorescence spectra of **D1** underwent a decrease in the intensity with a red-shift (ca. 27 nm) of the fluorescence band at around 450 nm in the water content region over 30 wt% (Fig. S27b, d, ESI†), and it is attributed to the formation of the hydrogen-bonded proton transfer complex (PTC) **D1-H$_2$O** with water molecules which shows a feeble fluorescence emission property, as well as the fluorescence solvatochromic property of **D1**.[19, 65] As with the case of **YNI-2-BF$_3$**, **D1-BF$_3$** exhibited a decrease in the ICT-based photoabsorption band at around 440 nm with a simultaneous increase in another ICT-based photoabsorption band at round 360 nm, and the appearance and enhancement of a fluorescence emission band at around 490 nm in the water content region below 20 wt%, which is attributed to the change in the ICT characteristics due to the dissociation of **D1-BF$_3$** into D-(π-A)$_2$-type pyridine dye **D1** (Fig. 5).[19] In addition, the absence of isosbestic point upon addition of water to the solution indicates the presence of the three or more chemical species (Fig. 5a, inset).[63, 64] Furthermore, in the high water content region over 25 wt%, a decrease in the fluorescence intensity was observed due to the formation of **D1-H$_2$O**. It is worth mentioning here that for **KOY-1** the photoabsorption band with $\lambda^{abs}_{max}$ at 366 nm showed a slight bathochromic shift, but at photoabsorption band with $\lambda^{abs}_{max}$ at 498 nm did not undergo

appreciable changes, upon addition of water to the acetonitrile solution (Fig. 6a, c). Meanwhile, the corresponding fluorescence spectra by the photoexcitation at 400 nm underwent a decrease in the intensity of the two fluorescence bands with the $\lambda^{fl}_{max}$ at 460 nm and the $\lambda^{fl}_{max}$ at 515 nm originating from the D-(π-A)$_2$ skeleton and the BODIPY skeleton, respectively, with the increase in the water content in the acetonitrile solution (Fig. 6b, d). On the other hand, the photoabsorption and fluorescence spectra of **A1** did not undergo appreciable changes upon the addition of water to the acetonitrile solution (Fig. S27e-h, ESI†). These results suggest that the resulting **KOY-1**, produced by adding water to the **KOY-1-BF$_3$** solution, may induce the formation of the hydrogen-bonded PTC **KOY-1-H$_2$O** with water molecules, which shows a feeble fluorescence emission property. Consequently, this results indicated that the amount of water over a wide range from low water content to high water content in solvents can be quantified by both the changes in absorbance at 438 nm originating from the ICT characteristics and fluorescence intensity at 515 nm originating from the BODIPY skeleton.

Furthermore, in order to investigate whether the optical response of **KOY-1-BF$_3$** is specific to water, we have performed the photoabsorption and fluorescence spectral measurements of **KOY-1-BF$_3$** in acetonitrile containing ethanol (0–40 wt%) as a protic solvent (Fig. S29, ESI†). It was fond that the changes in the photoabsorption and fluorescence spectra of **KOY-1-BF$_3$** upon the addition of ethanol are small compared to the case of the addition of water. This result demonstrated that ICT/FRET-type fluorescent sensor **KOY-1-BF$_3$** exhibits a somewhat selective optical response to water.

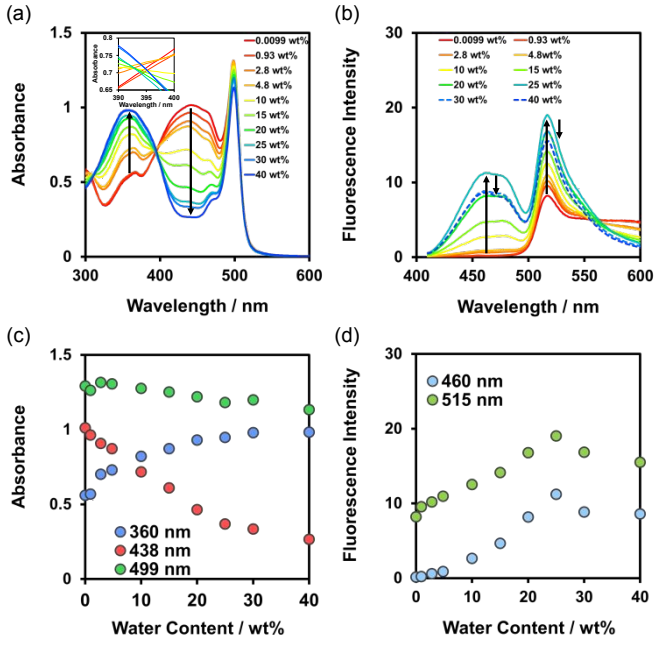


**Fig. 4** (a) Photoabsorption and (b) fluorescence spectra ($\lambda^{ex}$ = 400 nm) of **KOY-1-BF$_3$** ($c$ = 2.0×10$^{-5}$ M) in acetonitrile containing water (0.0099–40 wt%). (c) Absorbance at 360 nm, 438 nm and 499 nm of **KOY-1-BF$_3$** as a function of water content (0.0099–40 wt%) in acetonitrile. (d) Fluorescence peak intensity at 460 nm and 515 nm of **KOY-1-BF$_3$** ($\lambda^{ex}$ = 400 nm) as a function of water content (0.0099–40 wt%) in acetonitrile.

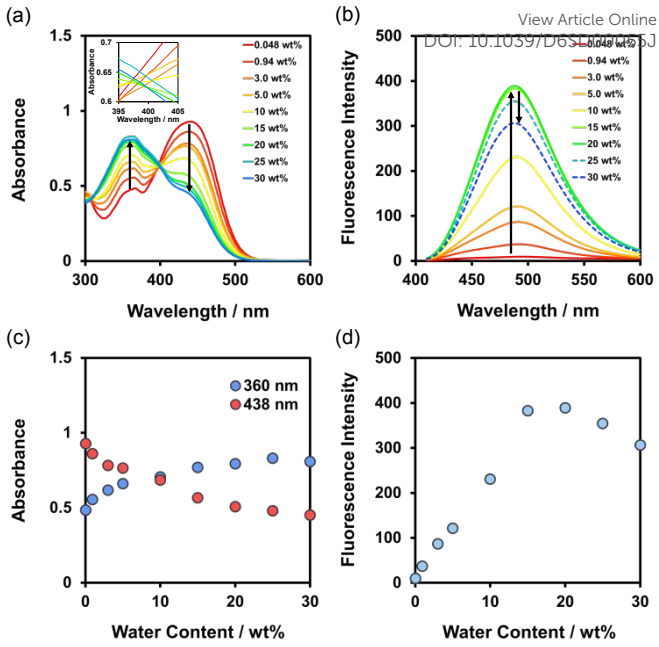


**Fig. 5** (a) Photoabsorption and (b) fluorescence spectra ($\lambda^{ex}$ = 400 nm) of **D1-BF$_3$** ($c$ = 2.0×10$^{-5}$ M) in acetonitrile containing water (0.048–30 wt%). (c) Absorbance at 360 nm and 438 nm of **D1-BF$_3$** as a function of water content (0.048–40 wt%) in acetonitrile. (d) Fluorescence peak intensity at 490 nm of **D1-BF$_3$** ($\lambda^{ex}$ = 400 nm) as a function of water content (0.048–40 wt%) in acetonitrile.

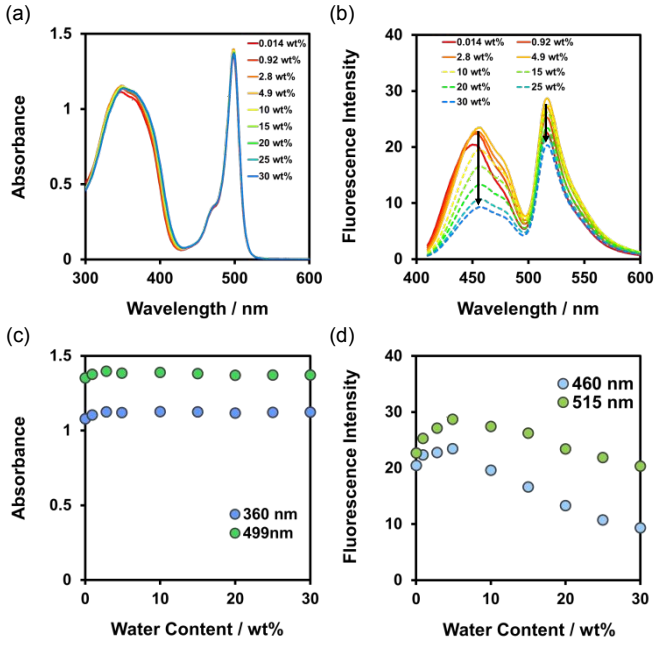


**Fig. 6** (a) Photoabsorption and (b) fluorescence spectra ($\lambda^{ex}$ = 400 nm) of **KOY-1** ($c$ = 2.0×10$^{-5}$ M) in acetonitrile containing water (0.014–40 wt%). (c) Absorbance at 360 nm and 499 nm of **KOY-1** as a function of water content (0.014–40 wt%) in acetonitrile. (d) Fluorescence peak intensity at 460 nm and 515 nm of **KOY-1** ($\lambda^{ex}$ = 400 nm) as a function of water content (0.014–40 wt%) in acetonitrile.

View Article Online
DOI: 10.1039/D6SD00051



On the basis of the above results, we considered the optical sensing ability of **KOY-1-BF$_3$** for water in acetonitrile. The $E_{FRET}$ value for **KOY-1-BF$_3$** in acetonitrile solution containing water content of 25 wt% corresponding to the maximum fluorescence intensity in the fluorescence enhancement process upon addition of water is estimated to be 49%, where $\tau_{DA}$ and $\tau_D$ are the fluorescence lifetimes of **KOY-1-BF$_3$** (0.85 ns) and **D1-BF$_3$** (1.68 ns), respectively, in acetonitrile containing water content of 25 wt% or 20 wt%. Indeed, the $E_{FRET}$ value (49%) is similar value with the case of **KOY-1** in the absolute acetonitrile solution ($E_{FRET}$ = 44%). Furthermore, the $E_{FRET}$ value (29%) for **KOY-1-BF$_3$** in acetonitrile solution containing water content of 40 wt% which corresponds to the minimum fluorescence intensity in the fluorescence attenuation process from the maximum fluorescence intensity upon addition of water, were estimated from the $\tau_{DA}$ value (0.77 ns) for **KOY-1-BF$_3$** and the $\tau_D$ value (1.08 ns) for **D1-BF$_3$** in acetonitrile containing water content of 40 wt% or 30 wt%. It is worth noting here that the $E_{FRET}$ value (29%) for **KOY-1-BF$_3$** in the acetonitrile solution containing water content of 40 wt% is lower than that (44%) for **KOY-1** in the absolute acetonitrile solution. Consequently, the fact doubtlessly indicates that the addition of water to **KOY-1-BF$_3$** solution causes its dissociation into thienylpyridine-carbazole-based D-(π-A)$_2$ fluorophore **KOY-1** and then the energy transfer from the excited-state donor fluorophore D-(π-A)$_2$ skeleton (**D1** structure) to acceptor fluorophore BODIPY skeleton (**A1** structure) through the FRET process, and thus resulting in a large pseudo-SS and an enhancement of fluorescence emission originating from BODIPY skeleton. As with case of **YNI-2-BF$_3$**, in the high water content region, the resulting **KOY-1** may induce the formation of the hydrogen-bonded proton transfer complex (PTC) **KOY-1-H$_2$O** with water molecules which shows a feeble fluorescence emission property, leading to a decrease in the fluorescence intensity due to the relatively low FRET efficiency, as well as the fluorescence solvatochromic property of **KOY-1**.

Thus, in order to estimate the sensitivity and accuracy characteristics of **KOY-1-BF$_3$** as a ICT/FRET-type fluorescent sensor for the detection of water in acetonitrile, the changes in fluorescence intensity at 460 nm and 515 nm are plotted against the water fraction below 25 wt% in acetonitrile (Fig. 7a). The plots demonstrated that the fluorescence peak intensity at 460 nm and 515 nm increased linearly as a function of the water content. Indeed, the correlation coefficient ($R^2$) values for the two calibration curves are 0.99 and 0.96, respectively, which indicates the good linearity. Therefore, the detection limit (DL) was determined from the plot of the fluorescence intensity at 460 nm and 515 nm versus water fraction in the low water content region below 25 wt% (DL = 3.3$\sigma$/$m_s$, where $\sigma$ is the standard deviation of the blank sample and $m_s$ is the slope of the calibration curve in the water content region below 25 wt%). The DL values for the fluorescence intensity at 460 nm and 515 nm are estimated to be 7.56 wt% and 8.27 wt%, respectively, that are inferior to that (0.14 wt%) of **D1-BF$_3$** (Fig. 7b) and those (0.018–0.25 wt%) of recently reported ICT-type, ESIPT-type, PET-type, FRET-type, and PET/FRET-type fluorescent sensors (Table S1, ESI†). The inferior DL value of **KOY-1-BF$_3$** may be attributed to the dynamic motion of phenylene spacer between donor (**D1** moiety) and acceptor (**A1** moiety) fluorophores, leading to the non-radiative decay of the photoexcited BODIPY fluorophore (**A1** moiety). In fact, the $\Phi_{fl}$ value (< 1%) of **KOY-1-BF$_3$** in acetonitrile with 25 wt% water content significantly is lower than that (12%) of **D1-BF$_3$** in acetonitrile with 15 wt% water content, although acceptor fluorophore **A1** shows moderate $\Phi_{fl}$ value (45%) in acetonitrile with and without water content. Thus, this result suggests that the DL values of ICT/FRET-type fluorescent sensor can be improved by using a rigid spacer such as an acetylene group to increase the $\Phi_{fl}$ value and by using a donor and acceptor fluorophores exhibiting good overlap integral of the donor fluorescence spectrum with the acceptor photoabsorption spectrum to enhance the FRET efficiency. Moreover, the ratio ($A_{360}/A_{438}$) of absorbance at 360 nm to that at 438 nm and the ratio ($Fl_{460}/Fl_{515}$) of fluorescence intensity at 460 nm to that at 515 nm are plotted against the water fraction below 40 wt% and 25 wt%, respectively, in acetonitrile (Fig. 7c, d). The two plots showed a good linear relationship with the $R^2$ values of 0.99, indicating ICT/FRET-type fluorescent sensor possessing large pseudo-SS is capable of detecting water in colorimetric and ratiometric fluorescent analysis. The fact also strongly indicates that the fluorescence sensing mechanism of **KOY-1-BF$_3$** for water is based on the change in the ICT characteristics and occurrence of FRET with the increase in the water content in solvent.

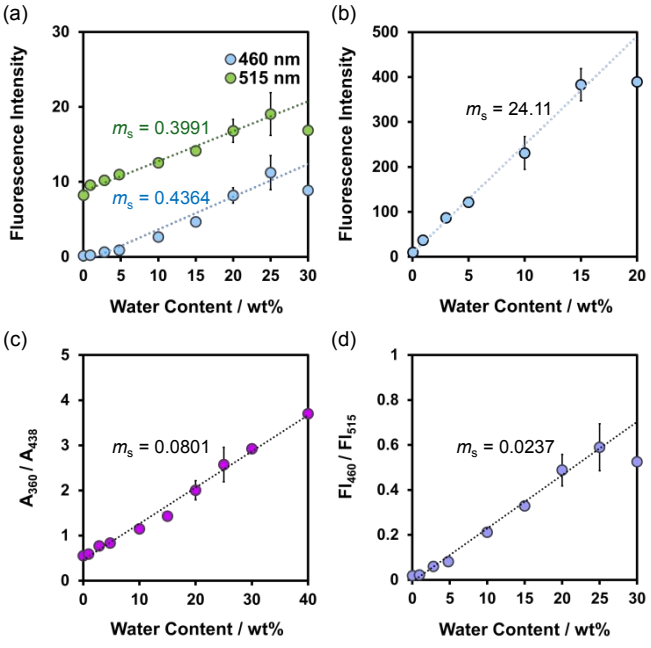


**Fig. 7** (a) Fluorescence peak intensity at 460 nm and 515 nm of **KOY-1-BF$_3$** ($\lambda^{ex}$ = 400 nm) as a function of water content below 25 wt% in acetonitrile. (b) Fluorescence peak intensity at 490 nm of **D1-BF$_3$** ($\lambda^{ex}$ = 400 nm) as a function of water content below 15 wt% in acetonitrile. (c) Ratio ($A_{360}/A_{438}$) of absorbance at 360 nm to that at 438 nm of **KOY-1-BF$_3$** as a function of water content below 40 wt% in acetonitrile. (d) Ratio ($Fl_{460}/Fl_{515}$) of fluorescence intensity at 460 nm to 515 nm of **KOY-1-BF$_3$** as a function of water content below 25 wt% in acetonitrile.

**Optical sensing mechanism for water**

In order to confirm the mechanism for detection of water in solvent based on the ICT/FRET characteristics of **KOY-1-BF$_3$**, we performed $^1$H and $^{11}$B NMR spectral measurement of **KOY-1-BF$_3$** and **KOY-1** with and without the addition of deuterium oxide ($D_2O$) in acetonitrile-$d_3$. For the $^1$H NMR spectrum of **KOY-1-BF$_3$** in acetonitrile-$d_3$ without the addition of $D_2O$ (Fig. 8a), it was observed that the chemical shifts of the aromatic protons on the two thienylpyridine moieties as well as the carbazole skeleton show a downfield shift compared to those for **KOY-1** in acetonitrile-$d_3$ without the addition of $D_2O$ (Fig. 8d), as with the cases of **YNI-2-BF$_3$** and **YNI-2** (Fig. 1). On the other hand, the $^1$H NMR spectrum of **KOY-1-BF$_3$** in acetonitrile-$d_3$ with $D_2O$ content of 25 wt% (Fig. 8b) which corresponds to the maximum fluorescence intensity in the fluorescence enhancement process, is similar to that of **KOY-1** in acetonitrile-$d_3$ without the addition of $D_2O$ (Fig. 8d). Indeed, this result demonstrates the dissociation of **KOY-1-BF$_3$** into **KOY-1** by water molecules. Moreover, the $^1$H NMR spectrum of **KOY-1-BF$_3$** in acetonitrile-$d_3$ with $D_2O$ content of 40 wt% (Fig. 8c) which corresponds to the fluorescence attenuation process from the maximum fluorescence intensity upon addition of water, is broadened, compared to that of **KOY-1-BF$_3$** in acetonitrile-$d_3$ with $D_2O$ content of 25 wt% (Fig. 8b), but is similar to that of **KOY-1** in the acetonitrile-$d_3$ solution with water $D_2O$ of 40 wt% (Fig. 8e). The $^1$H NMR spectrum of **KOY-1-BF$_3$** in acetonitrile-$d_3$ with water content of 40 wt% may indicate the existence of another chemical species in a polar protic solvent environment as well as the formation of **KOY-1**. In addition, the $^{11}$B NMR spectrum of **KOY-1-BF$_3$** showed that the signal (at around −0.6 ppm) of boron trifluoride ($BF_3$) coordinated to pyridine ring becomes relatively weaker than the signal (at around 1.3 ppm) of ($N_2BF_2$) in BODIPY skeleton with the increase in the $D_2O$ content (Fig. 9). It is wort noting here that with the addition of $D_2O$, the signal which is assignable to boric acid ($B(OD)_3$) that would be produced by the reaction of $BF_3$ with $D_2O$ appeared at around 20 ppm. This result also strongly indicates the dissociation of **KOY-1-BF$_3$** into **KOY-1** by water molecules.

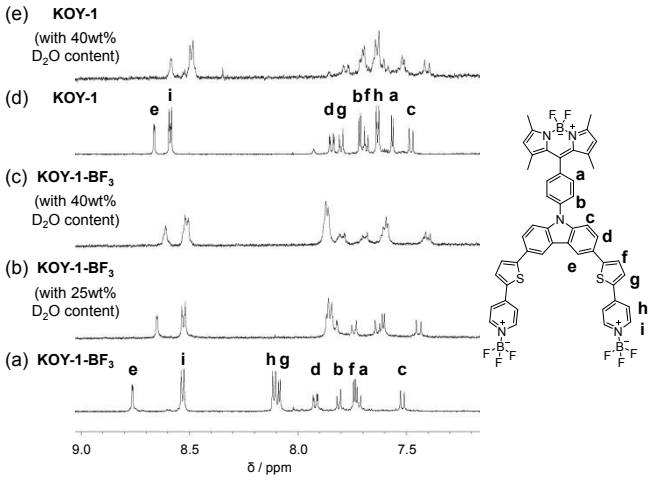


**Fig. 8** $^1$H NMR spectra of **KOY-1-BF$_3$** in acetonitrile-$d_3$ (a) without addition of $D_2O$, and with (b) 25 wt% and (c) 40 wt% $D_2O$ content. $^1$H NMR spectra of **KOY-1** in acetonitrile-$d_3$ (d) without addition of $D_2O$ and (e) with 40 wt% $D_2O$ content.

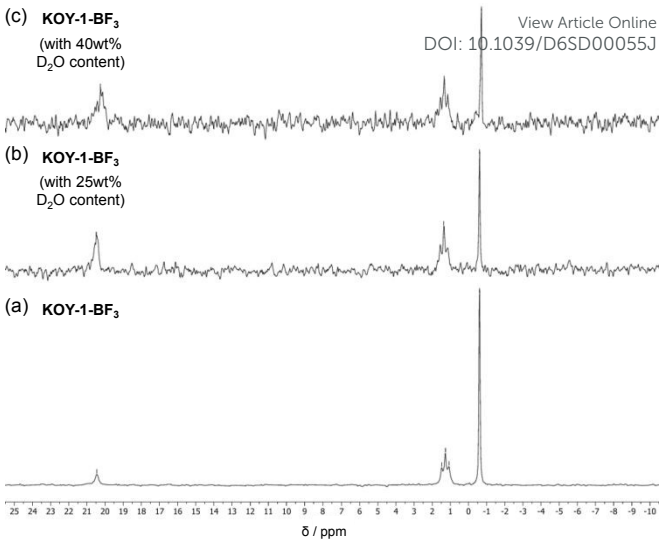


**Fig. 9** $^{11}$B NMR spectra of **KOY-1-BF$_3$** in acetonitrile-$d_3$ (a) without addition of $D_2O$, and with (b) 25 wt% and (c) 40 wt% $D_2O$ content.

Thus, the $^1$H and $^{11}$B NMR spectral measurements of **KOY-1-BF$_3$** in acetonitrile with and without the addition of water revealed that in the relatively low water content region **KOY-1-BF$_3$** causes its dissociation into thienylpyridine-carbazole-based D-($\pi$-A)$_2$-BODIPY fluorophore **KOY-1** and $BF_3$ (Fig. 10), resulting in the blue-shift of ICT-based photoabsorption and the enhancement of fluorescence emission originating from BODIPY skeleton through the FRET process between the excited-state donor fluorophore D-($\pi$-A)$_2$ skeleton and acceptor fluorophore BODIPY skeleton. In this experimental condition we could not detect the chemical species with mono pyridine-$BF_3$ unit which may be formed by the dissociation of one $BF_3$ unit from **KOY-1-BF$_3$**. Thus, the fact suggests that **KOY-1** is more stable than the chemical species with mono pyridine-$BF_3$ unit, leading to rapid and preferential dissociation of **KOY-1-BF$_3$** into **KOY-1**, as with the case of **YNI-2-BF$_3$**.[19] Moreover, in the relatively high water content region, the resulting **KOY-1** induces the formation of the hydrogen-bonded proton transfer complex (PTC) **KOY-1-H$_2$O** between the pyridinic nitrogen atom of **KOY-1** and the hydroxyl group of water molecules (Fig. 10). Thus, the decrease in fluorescence intensity in the relatively high water content region is attributed to not only the formation of **KOY-1-H$_2$O** which shows a feeble fluorescence emission property, but also the fluorescence solvatochromism due to the ICT characteristics of **KOY-1**, leading to a relatively low FRET efficiency. In addition, the absence of isosbestic point in the photoabsorption spectra with the increase in the water content also indicates the presence of the three or more chemical species[63, 64], that is, **KOY-1** and **KOY-1-H$_2$O**.

As shown in Fig. 10, the color of **YNI-2-BF$_3$** in acetonitrile is orange. Upon the addition of water, the solution changed from orange to nearly colorless due to the dissociation of **KOY-1-BF$_3$** into **KOY-1**. Meanwhile, fluorescent color for the absolute acetonitrile solution of **KOY-1-BF$_3$** seems yellow fluorescence, but the solution containing water content exhibited intense light blue fluorescence emission originating from the thienylpyridine-

carbazole-based D-(π-A)$_2$ and BODIPY skeletons due to the formation of **KOY-1**. However, the acetonitrile solution with the high water content shows greenish blue fluorescence emission due to the relatively low FRET efficiency by the hydrogen-bonded PTC (**KOY-1-H$_2$O**) with water molecules as well as the fluorescence solvatochromic property of **KOY-1**. Consequently, this work demonstrates that **KOY-1-BF$_3$** composed of an ICT-type donor fluorophore and an acceptor fluorophore in the FRET process can act as a colorimetric and fluorescent sensor based on ICT/FRET mechanism for detection of water over a wide range from low water content to high water content in solvents.

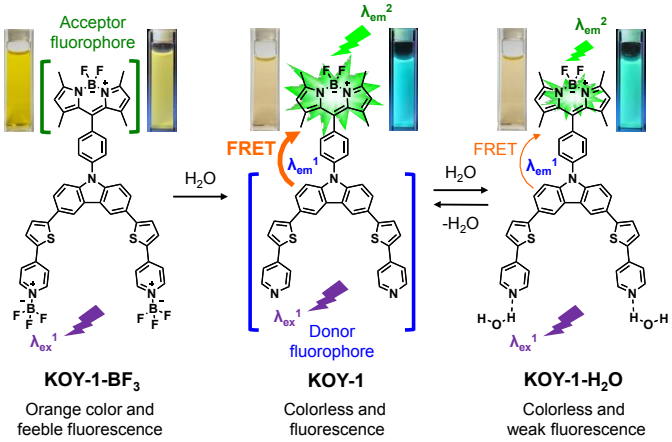


**Fig. 10** Proposed mechanisms of ICT/FRET-type colorimetric and fluorescent sensor **KOY-1-BF$_3$** for the detection of water in solvent; inset: color (left) and fluorescence color (right) images (under 365 nm irradiation).

## Conclusions

We have newly designed and developed a ICT/FRET-type colorimetric and fluorescent sensor **KOY-1-BF$_3$** possessing a large pseudo-SS for detection of water in solvents; **KOY-1-BF$_3$** is composed of a ICT-type donor fluorophore (thienylpyridine-carbazole-based D-(π-A)$_2$ skeleton) and an acceptor fluorophore (BODIPY skeleton) in the FRET process. It was found that in the low water content region **KOY-1-BF$_3$** causes its dissociation into thienylpyridine-carbazole-based D-(π-A)$_2$-BODIPY fluorophore **KOY-1** and $BF_3$, leading to the blue-shift of ICT-based photoabsorption band due to the change in the ICT characteristics and enhancement of fluorescence emission originating from BODIPY skeleton by occurrence of FRET from the excited-state donor fluorophore D-(π-A)$_2$ skeleton to acceptor fluorophore BODIPY skeleton. Moreover, the decrease in fluorescence intensity in the high water content region is attributed to not only the formation of the hydrogen-bonded proton transfer complex (PTC) **KOY-1-H$_2$O** with water molecules which shows a feeble fluorescence emission property, but also the fluorescence solvatochromism due to the ICT characteristics of **KOY-1**, leading to a relatively low FRET efficiency. Consequently, it was demonstrated that the ICT/FRET-type colorimetric and fluorescent sensor **KOY-1-BF$_3$** possesses a large pseudo-SS of 7942 cm$^{-1}$ (150 nm) and moderate FRET efficiency (49%). We anticipate that this work will provide one of the most promising fluorescence enhancement (turn-on) system with a large Stokes shift for detection of water and lead to creation of functional materials as well as colorimetric and fluorescent method to enable visualization and quantification of water.

## Author Contributions

Y.O. conceived the project. K.I. directed the experimental work. K.O. performed most of the experiments.

## Conflicts of interest

The authors declare that there are no conflicts of interest.

## Data availability

The data that support the findings of this work are available in supplementary information (SI). Supplementary Information: details of the experimental methods, additional figures and tables.

## Acknowledgements

This work was supported by the Japan Society for the Promotion of Science (JSPS) KAKENHI Grant Number 25K01808 and 25K22857 and by Toshiaki Ogasawara Memorial Foundation.

## References

1 R. Wernecke, and J. Wernecke, *Industrial Moisture and Humidity Measurement*, Wiley-VCH, Weinheim, 2013.
2 L.-O. Nilsson, *Methods of Measuring Moisture in Building Materials and Structures*, Springer, Switzerland, 2018.
3 M. Liu, X. Zheng, M. Zhang, S. Yao, P. Zhang, L. Lianga and Y. C. Chen, *Chem. Commun.*, 2026, **62**, 1572–1575.
4 M. Chandrakanth, Fabitha K, C. A. Swamy P and J. Banothu, *New J. Chem.*, 2026, **50**, 3026–3036.
5 J. Issac, R. R. Priyadharsan, K. Chidambaranathan, S. Karthikeyan, D. Moon, S. P. Anthony and V. Madhu, *RSC Adv.*, 2025, **15**, 44205–44212.
6 Y. Ida, K. Imato and Y. Ooyama, *New J. Chem.*, 2025, **49**, 19950–19954.
7 D. Han, H. Liu, Y. Liu, Y. Zhang, G. Suna and J. Wang, *New J. Chem.*, 2025, **49**, 12523–12531
8 S. Mishra and A. K. Singh, *Coord. Chem. Rev.*, 2021, **445**, 214063.
9 H. S. Jung, P. Verwilst, W. Y. Kim and J. S. Kim, *Chem. Soc. Rev.*, 2016, **45**, 1242–1256.
10 P. P. Dash, A. K. Ghosh, P. Mohanty, R. Behura, S. Behera, B. R. Jali and S. K. Sahoo, *Talanta*, 2024, **275**, 126089.
11 W.-E. Lee, Y.-J. Jin, L.-S. Park and G. Kwak, *Adv. Mater.*, 2012, **24**, 5604–5609.
12 J. Lee, M. Pyo, S. Lee, J. Kim, M. Ra, W.-Y. Kim, B. J. Park, C. W. Lee and J.-M. Kim, *Nat. Commun.*, 2014, **5**, 3736.
13 A. Morimoto, K. Shimizu, N. Suzuki, S. Yagi, K. Sueyoshi, T. Endo and H. Hisamoto, *Analyst*, 2024, **149**, 1939–1946.
14 G. Das, F. A. Ibrahim, Z. A. Khalil, P. Bazin, F. Chandra, R. G. AbdulHalim, T. Prakasam, A. K. Das, S. K. Sharma, S. Varghese, S. Kirmizialtin, R. Jagannathan, N. Saleh, F. Benyettou, M. E. Roz, M. Addicoat, M. A. Olson, D. S. S. Rao, S. K. Prasad and A. Trabolsi, *Small*, 2024, **20**, 2311064.

15 J. Wang, Y. Huang, Z. Gao and J. Du, *ACS. Appl. Nano Mater.*, 2024, **7**, 7958–7965.
16 I. M. Resta and F. Galindo, *Dyes Pigm.*, 2022, **197**, 109908.
17 Z. Zhao, Q. Hu, W. Liu, X. Xiong, Z. Wang and H. Wang, *Dyes Pigm.*, 2023, **213**, 111186.
18 K. P. Jose, R. R. Priyadharsan, K. Chidambaranathan, S. Karthikeyan, S. P. Anthony, V. Madhu, *Dyes Pigm.*, 2025, **242**, 112926.
19 S. Tsumura, T. Enoki and Y. Ooyama, *Chem. Commun.*, 2018, **54**, 10144–10147.
20 T. Enoki and Y. Ooyama, *Dalton Trans.*, 2019, **48**, 2086–2092.
21 K. Imato, T. Enoki and Y. Ooyama, *RSC Adv.*, 2019, **9**, 31466–31473.
22 Y. Dai, H. Gao and H. Huang, *Anal. Methods*, 2025, **17**, 9823–9832.
23 A. Ghosh, A. Adhikary and S. Guria, *Chem. Asian J.*, 2025, **20**, e00778.
24 Y. Hong, C. Cui, S. Li, Z. Yan, Q. Zhou, K. Li and Z. Wang, *Anal. Methods*, 2025, **17**, 7033–7045.
25 D. Han, H. Liu, Y. Liu, Y. Zhang, G. Suna and J. Wang, *New J. Chem.*, 2025, **49**, 12523–12531.
26 J. S. Kim, M. G. Choi, Y. Huh, M. H. Kim, S. H. Kim, S. Y. Wang and S.-K. Chang, *Bull. Korean Chem. Soc.*, 2006, **27**, 2058–2060.
27 A. C. Kumar and A. K. Mishra, *Talanta*, 2007, **71**, 2003–2006.
28 Y. Ooyama, *Sustainable and Functional Redox Chemistry* (Ed. Inagi, S.), the Royal Society of Chemistry, Cambridge, UK, Chap.13, 300–330, 2022.
29 Y. Ooyama, M. Sumomogi, T. Nagano, K. Kushimoto, K. Komaguchi, I. Imae and Y. Harima, *Org. Biomol. Chem.*, 2011, **9**, 1314–1316.
30 Y. Ooyama, A. Matsugasako, K. Oka, T. Nagano, M. Sumomogi, K. Komaguchi, I. Imae and Y. Harima, *Chem. Commun.*, 2011, **47**, 4448–4450.
31 Y. Ooyama, A. Matsugasako, Y. Hagiwara, J. Ohshita and Y. Harima, *RSC Adv.*, 2012, **2**, 7666–7668.
32 Y. Ooyama, K. Furue, K. Uenaka and J. Ohshita, *RSC Adv.*, 2014, **4**, 25330–25333.
33 Y. Ooyama, M. Hato, T. Enoki, S. Aoyama, K. Furue, N. Tsunoji and J. Ohshita, *New J. Chem.*, 2016, **40**, 7278–7281.
34 Y. Ooyama, R. Sagisaka, T. Enoki, N. Tsunoji and J. Ohshita, *New J. Chem.*, 2018, **42**, 13339–13350.
35 D. Jinbo, K. Imato and Y. Ooyama, *RSC Adv.*, 2019, **9**, 15335–15340.
36 D. Jinbo, K. Ohira, K. Imato and Y. Ooyama, *Mater. Adv.,* 2020, **1**, 354–362.
37 Y. Mise, K. Imato, T. Ogi, N. Tsunoji and Y. Ooyama, *New J. Chem.,* 2021, **45**, 4164–4173.
38 T. Fumoto, S. Miho, Y. Mise, K. Imato and Y. Ooyama, *RSC. Adv.,* 2021, **11**, 17046–17050.
39 S. Miho, T. Fumoto, Y. Mise, K. Imato, S. Akiyama, M. Ishida and Y. Ooyama, *Mater. Adv.,* 2021, **2**, 7662–7670.
40 E. Nishimoto, Y. Mise, T. Fumoto, S. Miho, N. Tsunoji, K. Imato and Y. Ooyama, *New*, *J. Chem.*, 2022, **46**, 12474–12481.
41 S. Miho, K. Imato and Y. Ooyama, *RSC. Adv.,* 2022, **12**, 25687–25696.
42 T. Fumoto, K. Imato and Y. Ooyama, *New*, *J. Chem.*, 2022, **46**, 21037–21046.
43 K. Tao, K. Imato and Y. Ooyama, *Sens. Diagn.*, 2024, **3**, 631–639.
44 C. C. Ghosh and P. P. Parui, *New J. Chem.*, 2025, **49**, 10420–10428.
45 Di Yang, Xiao-Tian Wu, Xiang-Jian Cao, Bao-Xiang Zhao, *Dyes Pigm.*, 2019, **170**, 107558.
46 D. Han, H. Liu, Y. Liu, Y. Zhang, G. Suna and J. Wang, *New J. Chem.*, 2025, **49**, 12523–12531.
47 F. Khan, A. Ekbote, S. M. Mobin and R. Misra, *J. Org. Chem.*, 2021, **86**, 1560–1574.
48 X. Y. Shen, Y. J. Wang, H. Zhang, A. Qin, J. Z. Sun and B. Z. Tang, *Chem. Commun.*, 2014, **50**, 8747–8750.
49 L. Ding, Z. Zhang, X. Li and J. Su, *Chem. Commun.*, 2013, **49**, 7319–7321.
50 Y. Mise, K. Imato, T. Ogi, N. Tsunoji and Y. Ooyama, *New J. Chem.,* 2021, **45**, 4164–4173.
51 Y. Zhang, D. Li, Y. Li and J. Yu, *Chem. Sci.*, 2014, **5**, 2710–2716.
52 N. Zhao, Z. Yang, J. W. Y. Lam, H. H. Y. Sung, N. Xie, S. Chen, H. Su, M. Gao, I. D. Williams, K. S. Wong and B. Z. Tang, *Chem. Commun.,* 2012, **48**, 8637–8639.
53 K. M. Meghna, M. M. A. Kumar, S. Sarkar and V. M. Biju, *Anal. Methods*, 2026, **18**, 372–388.
54 L. He, B. Dong, Y. Liu and W. Lin, *Chem. Soc. Rev*, 2016, **45**, 6449–6461.
55 F. Peng, X. Ai, J. Sun, L. Yang and B. Gao, *Chem. Commun*, 2024, **60**, 2994–3007.
56 Y. Xu, B. Hu, Y. Cui, L. Li, F. Nian, Z. Zhang and W. Wang, *Chem. Commun*, 2024, **60**, 83–86.
57 Z. Tang, H. Huang, Y. Yao, S. Gao, B. Lin, Q. Zong, W. Hu, J. Xu, Y. Wand and L. Guo, *Chem. Commun*, 2025, **61**, 560–563.
58 K. Xu, L. He, X. Yang, Y. Yand and W. Lin, *Analyst*, 2018, **143**, 3555–3559.
59 L.-K. Li, Y.-M. Hou, X.-C. Liu, M.-J. Tian, Q.-J. MA, N.-N. Zhu and S.-Z. Liu, *New J. Chem.*, 2022, **46**, 6596–6602.
60 W. Zhang, F. Huo, F. Cheng and C. Yin, *J. Am. Chem. Soc.*, 2020, **142**, 6324–6331.
61 F. Xu, J.-H. Kim, H. U. Kim, J.-H. Jang, K. S. Yook, J. Y. Lee and D.H. Hwang, *Macromolecules*, 2014, **47**, 7397−7406.
62 Y. Ooyama, S. Inoue, T. Nagano, K. Kushimoto, J. Ohshita, I. Imae, K. Komaguchi and Y. Harima, *Angew. Chem. Int. Ed.*, 2011, **50**, 7429−7433.
63 M. D. Cohen and E. Fischer, *J. Chem. Soc.*, 1962, 3044−3052.
64 J. Brynestad and G. P. Smith, *J. Phys. Chem.*, 1968, **72**, 296−300.
65 C. Reichardt, *Solvents and Solvent Effects in Organic Chemistry*, VCH, Weinheim, 2003.

View Article Online
DOI: 10.1039/D6SD00055J

## Data availability

The data that support the findings of this work are available in supplementary information (SI). Supplementary Information: details of the experimental methods, additional figures and tables.